

Outbreaks in susceptible-infected-removed epidemics with multiple seedsTakehisa Hasegawa^{1,*} and Koji Nemoto^{2,†}¹*Department of Mathematics and Informatics, Ibaraki University, 2-1-1 Bunkyo, Mito 310-8512, Japan*²*Department of Physics, Hokkaido University, Kita 10, Nishi 8, Kita-ku, Sapporo 060-0810, Japan*

(Received 29 October 2015; revised manuscript received 5 March 2016; published 30 March 2016)

We study a susceptible-infected-removed (SIR) model with multiple seeds on a regular random graph. Many researchers have studied the epidemic threshold of epidemic models above which a global outbreak can occur, starting from an infinitesimal fraction of seeds. However, there have been few studies of epidemic models with finite fractions of seeds. The aim of this paper is to clarify what happens in phase transitions in such cases. The SIR model in networks exhibits two percolation transitions. We derive the percolation transition points for the SIR model with multiple seeds to show that as the infection rate increases epidemic clusters generated from each seed percolate before a single seed can induce a global outbreak.

DOI: [10.1103/PhysRevE.93.032324](https://doi.org/10.1103/PhysRevE.93.032324)**I. INTRODUCTION**

The threat of infectious disease is becoming increasingly conspicuous for modern society, wherein there is a large amount of international travel all over the world. Understanding how infectious diseases spread in our society is crucial to the development of strategies for disease control. A mathematical model of infectious disease, called the susceptible-infected-removed (SIR) model, was first applied with the assumption of a well-mixed population for computation of the final numbers of infected and eventually removed (or recovered) individuals [1]. So far, many mathematical models of infectious diseases have been proposed for understanding the spread of epidemics and proposing strategies for disease control [2].

In recent years, many studies have been devoted to epidemic models with a network structure of people [3]. Diseases spread over the networks of physical contacts between individuals, and the structure of real networks [4–7] has crucial effects on this spread. For example, Moreno *et al.* [8] studied the SIR model in a scale-free network having a degree distribution of $p_k \propto k^{-\gamma}$ using a degree-based mean-field approach. Their approximation clarified that epidemics can spread over the network for any infection rate if $\gamma \leq 3$. In addition, many analytical approaches for epidemic models with network structures, such as the approximation onto a bond percolation problem [9,10], the edge-based compartment model [11], the effective degree approach [12], and the pair approximation [13,14], have been proposed and have succeeded in describing epidemic dynamics. Numerical simulations have revealed how epidemics spread in more realistic situations. Also, several strategies for disease control have been proposed on the basis of the knowledge of epidemics on networks, e.g., target immunization [15,16], acquaintance immunization [16–19], and graph-partitioning immunization [20].

Most previous studies using SIR-type epidemic models have assumed that the fraction of infection seeds is infinitesimally small. In contrast, there have been few studies on epidemic models with finite fractions of seeds. Miller [21] considered the SIR model in networks with large initial

conditions to resolve an apparent paradox in works assuming an infinitesimal fraction of seeds. Hu *et al.* [22] numerically studied how the positions of multiple seeds in a network affect spreading behavior. Ji *et al.* [23] identified multiple influential spreaders in real networks by ranking nodes in disintegrated networks after random bond removals. What we discuss here is a more fundamental, but almost overlooked problem: How do epidemic models with finite fractions of seeds undergo phase transitions? For SIR-type epidemics, each infection seed creates an epidemic cluster of infected individuals. Epidemic clusters generated by multiple seeds will have global connectivity in some parameter regions even though each seed may not have the potential to induce a global outbreak there.

In this paper, we consider the SIR model in networks with multiple seeds. In this case, the SIR model exhibits a kind of percolation transition. An epidemic cluster grows from each of multiple seeds. We regard the clusters so generated as *supernodes* and study the percolation problem of these supernodes. Indeed, we can analytically and numerically obtain the percolation transition point of supernodes to show a gap between this transition point and the epidemic threshold. The existence of this gap indicates that the percolation transition of epidemic clusters occurs before a single seed can induce a global outbreak. Our result also shows the sensitivity of the seed fraction on percolation transition points, i.e., that a small seed fraction drastically reduces the critical infection rate for the emergence of the infinite epidemic cluster.

II. MODEL

Let us give a brief review of the SIR model in a given static network. Each node in the network takes one of three states: susceptible, infected, and removed. The system evolves as a continuous-time Markov process. As an initial-state configuration, a fraction, ρ , of the nodes is randomly chosen to be seeds and is initially infected, while other nodes are susceptible. The infection rate is denoted by λ . When an infected node is adjacent to a susceptible node, this susceptible node gets infected with probability $\lambda\Delta t$ within a short time, Δt . Note that this probability is independently given by each of the infected nodes so that the total infection rate at a node is just proportional to the number of infected neighbors. An infected

*takehisa.hasegawa.sci@vc.ibaraki.ac.jp

†nemoto@statphys.sci.hokudai.ac.jp

node becomes removed at a rate μ , i.e., with probability $\mu \Delta t$ within a short time Δt , irrespective of the neighbors' states. Without loss of generality, we set $\mu = 1$ unless otherwise specified. The dynamics stops when no infected nodes exist in the network.

Let us consider the limit $\rho \rightarrow 0$. The SIR model exhibits a phase transition at the epidemic threshold $\lambda = \lambda_c^{\text{SIR}}$ when λ increases from 0. Above λ_c^{SIR} , a single seed can induce global outbreaks. In a global outbreak, a nonzero fraction of nodes become infected and eventually removed. Below λ_c^{SIR} , the number of removed nodes is always negligible compared with the total number of nodes. As already mentioned, we have several approaches for obtaining λ_c^{SIR} (see the recent review [3]); Newman approximated the SIR model in uncorrelated networks by mapping onto a bond percolation problem (which is called the SIR model with transmissibility) [10] and derived λ_c^{SIR} as

$$\lambda_c^{\text{SIR}} = \frac{\langle k \rangle}{\langle k^2 \rangle - 2\langle k \rangle}, \quad (1)$$

where $\langle k \rangle$ and $\langle k^2 \rangle$ are the first and the second moments of the degree distribution, p_k , respectively [24]. This result indicates that, for a fat-tailed scale-free network whose degree distribution obeys $p_k \propto k^{-\gamma}$ with $\gamma \leq 3$, a global outbreak starting from an infinitesimal fraction of seeds occurs even for an infinitesimal infection rate. As indicated in [25], mapping onto a bond percolation problem does not give the exact outbreak size or probability, but it does predict exactly the epidemic threshold. Lindquist *et al.* [12] proposed an effective degree approach for describing the time evolution of the SIR dynamics using numerous ordinary differential equations and derived the same epidemic threshold, (1). Miller [11] introduced another approach by means of the edge-based compartment model to enable accurate descriptions of the SIR dynamics accurately with a few rate equations.

We can also describe the phase transition of the present model in terms of percolation. In any final state, each node takes either a susceptible or a removed state. We call the connected components of removed nodes and susceptible nodes the R components and the S components, respectively. For the SIR model in networks with $\rho \gtrsim 0$, we have two percolation transition points, λ_{c1} and λ_{c2} . When the number of nodes, N , is much greater than 1, the mean fraction of the largest R component, $r_{\max}(N) = R_{\max}(N)/N$, where $R_{\max}(N)$ is the mean size of the largest R component, changes from 0 to a nonzero value at the former point λ_{c1} . Note that λ_{c1} corresponds to λ_c^{SIR} in the limit $\rho \rightarrow 0$ by definition. Percolation analysis of an epidemic cluster starting from a single seed has been used for numerical computations of the epidemic threshold and critical properties [26,27]. The latter point, λ_{c2} , is on the percolation of the S component (also called the residual graph [28,29]) and is usually larger than λ_{c1} . Above λ_{c2} , the network remaining after removal of the R components is disintegrated such that the sizes of all remaining components are finite. In other words, the mean fraction of the largest S component, $s_{\max}(N) = S_{\max}(N)/N$, where $S_{\max}(N)$ is the mean largest S-component size, is 0 (nonzero) for $\lambda > \lambda_{c2}$ ($\lambda < \lambda_{c2}$) when $N \gg 1$. Whether the susceptible nodes are globally connected is important because

a second epidemic spread may occur in the remaining network [28,30]. In [28], Newman analyzed this second transition point of the SIR model with transmissibility in uncorrelated networks with $\rho \rightarrow 0$ to show that the transition point is positive even when $\gamma \leq 3$. Valdez *et al.* [31] proposed a new strategy for suppressing epidemics by regarding this second transition point as a measure of the efficiency of a mitigation or control strategy. If we regard the present model as showing the propagation of an attack against a network, such as a computer virus, λ_{c2} is a measure of the robustness of networks against such attacks [32,33]. Konno and the authors numerically studied λ_{c2} for correlated networks to show that any positive or negative degree correlation makes networks more robust [33].

To summarize, the system with a given value of ρ has the following three regions: (i) the S-dominant phase, where $r_{\max} = 0$ and $s_{\max} > 0$ for $\lambda < \lambda_{c1}$; (ii) the coexisting phase, where $r_{\max} > 0$ and $s_{\max} > 0$ for $\lambda_{c1} < \lambda < \lambda_{c2}$; and (iii) the R-dominant phase, where $r_{\max} > 0$ and $s_{\max} = 0$ for $\lambda > \lambda_{c2}$. To investigate in detail the phase transitions of the SIR model with a finite fraction of seeds, we focus on the z -regular random graph (RRG). Our formulations discussed below are for the RRG. The extension to degree-uncorrelated networks having degree distribution $p(k)$ may be straightforward, although its execution will be cumbersome. At any rate, our findings obtained from the RRG probably will be in common with other networks. In Sec. IV D, we numerically study the outbreaks induced by multiple seeds in finite-dimensional Euclidean lattices.

III. TOTAL DENSITIES OF SUSCEPTIBLE AND REMOVED NODES

To evaluate the time evolution of the SIR dynamics and the total densities of the susceptible and removed nodes in the final states, we consider the approximate master equations (AMEs) [12,14]. Let $s_{l,m}(t)$, $i_{l,m}(t)$, and $r_{l,m}(t)$ be the fractions of nodes that are susceptible, infected, and removed, respectively, at time t and have l susceptible and m infected neighbors. The AMEs for the evolution of these variables are as follows (see [12] for details):

$$\begin{aligned} \dot{s}_{l,m} = & -\lambda m s_{l,m} + \beta_s^{si} [(l+1)s_{l+1,m-1} - l s_{l,m}] \\ & + \beta_s^{ir} [(m+1)s_{l,m+1} - m s_{l,m}], \end{aligned} \quad (2)$$

$$\begin{aligned} \dot{i}_{l,m} = & \lambda m s_{l,m} - \mu i_{l,m} + \beta_i^{si} [(l+1)i_{l+1,m-1} - l i_{l,m}] \\ & + \beta_i^{ir} [(m+1)i_{l,m+1} - m i_{l,m}], \end{aligned} \quad (3)$$

$$\begin{aligned} \dot{r}_{l,m} = & \mu i_{l,m} + \beta_r^{si} [(l+1)r_{l+1,m-1} - l r_{l,m}] \\ & + \beta_r^{ir} [(m+1)r_{l,m+1} - m r_{l,m}]. \end{aligned} \quad (4)$$

The transition rates of neighboring nodes are approximated as

$$\beta_s^{si} = \lambda \frac{\sum_{l,m} l m s_{l,m}}{\sum_{l,m} l s_{l,m}}, \quad \beta_s^{ir} = \mu \frac{\sum_{l,m} l i_{l,m}}{\sum_{l,m} l i_{l,m}} = \mu, \quad (5)$$

$$\beta_i^{si} = \lambda \frac{\sum_{l,m} m^2 s_{l,m}}{\sum_{l,m} m s_{l,m}}, \quad \beta_i^{ir} = \mu \frac{\sum_{l,m} m i_{l,m}}{\sum_{l,m} m i_{l,m}} = \mu, \quad (6)$$

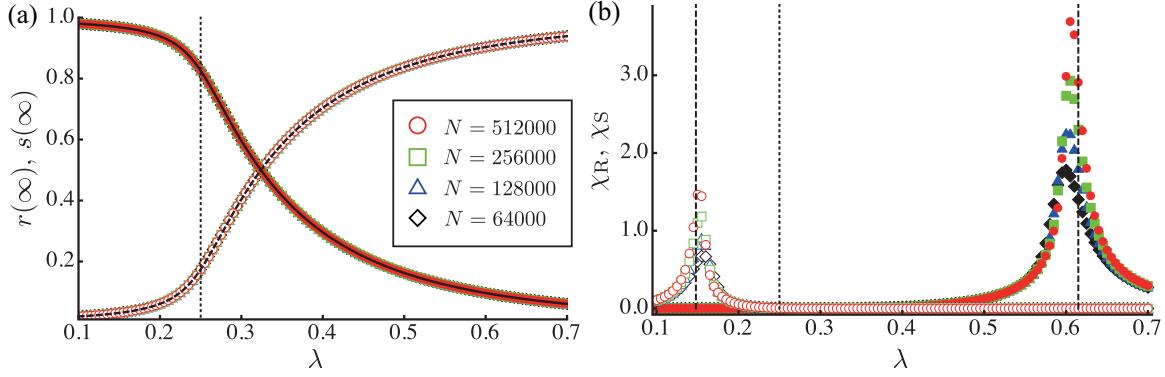


FIG. 1. Numerical results for the SIR model with $\rho = 0.01$ on the RRG: (a) total densities of the removed nodes r (open symbols) and of the susceptible nodes s (filled symbols) and (b) susceptibility of the R components χ_R (open symbols) and of the S components χ_S (filled symbols). The dashed and solid lines in (a) are drawn from the AMEs. In (b), the dotted vertical line represents λ_c^{SIR} , and the two dashed vertical lines represent $\lambda_{c1} = 0.148$ and $\lambda_{c2} = 0.615$, which are given in Sec. IV.

$$\beta_r^{si} = \lambda \frac{\sum_{l,m} (k-l-m) m s_{l,m}}{\sum_{l,m} (k-l-m) s_{l,m}}, \quad \beta_r^{ir} = \mu, \quad (7)$$

where the summations run over all $0 \leq l + m \leq k$. To describe the SIR dynamics with $\rho > 0$, we set the initial condition as

$$s_{l,m}(0) = \delta_{k,l+m} (1 - \rho) \binom{k}{l} (1 - \rho)^l \rho^m, \quad (8)$$

$$i_{l,m}(0) = \delta_{k,l+m} \rho \binom{k}{l} (1 - \rho)^l \rho^m, \quad (9)$$

$$r_{l,m}(0) = 0. \quad (10)$$

By numerical evaluation of the above equations, we obtain the total densities

$$s(t) = \sum_{l,m} s_{l,m}(t), \quad i(t) = \sum_{l,m} i_{l,m}(t), \quad r(t) = \sum_{l,m} r_{l,m}(t), \quad (11)$$

which satisfy the conservation law,

$$s(t) + i(t) + r(t) = 1, \quad (12)$$

at any time t . Note that all variables other than $s_{l,0}$ and $r_{l,0}$ vanish in the limit $t \rightarrow \infty$, and therefore $i(\infty) = 0$.

To check the accuracy of the AME, we perform Monte Carlo simulations for the SIR model on the RRG with $z = 6$. In our simulations, we set $\mu = 1$ and $\rho = 0.01$. The numbers of nodes are $N = 64\,000$, $128\,000$, $256\,000$, and $512\,000$. The number of graph realizations is 100, and the number of trials on each graph is 500. Figure 1(a) shows the AME result (line) and the Monte Carlo result (symbols) of the total densities of susceptible and removed nodes, s and r , in the final states. We find that data from the AMEs wholly coincide with those from the Monte Carlo simulations.

Equations (2)–(11) do not predict any transition point for $\rho > 0$ because $r(\infty) \geq \rho > 0$, although it is possible to derive the epidemic threshold $\lambda_c^{\text{SIR}} = \mu/(z - 2)$ for the RRG with degree z [12] by considering the limit $\rho \rightarrow 0$ (see Appendix A). In contrast, the Monte Carlo simulations suggest that the model actually exhibits phase transitions. In Fig. 1(b), we plot the

R and S susceptibilities (which we call the susceptibility by analogy with the magnetic susceptibility in spin systems) χ_R and χ_S . Here, χ_R (χ_S) is defined as the mean size of all R components (S components) except the largest one [34]. We find that χ_R and χ_S have peaks at λ_{c1} and λ_{c2} , respectively, implying two phase transitions. Moreover, these points are clearly different from λ_c^{SIR} . In particular, the gap between λ_{c1} and λ_c^{SIR} indicates that as the infection rate increases, the epidemic clusters generated from each seed percolate before a single seed can induce a global outbreak. In the next section, we derive these percolation transition points for $0 < \rho < 1$.

IV. PERCOLATION TRANSITIONS OF THE SIR DYNAMICS WITH MULTIPLE SEEDS

A. Derivation of λ_{c2}

To derive λ_{c2} , we consider the percolation of the S components. In [28], Newman analyzed the percolation of the S components using generating functions. His method gives λ_{c2} for the SIR model in uncorrelated networks but assumes a single seed. By combining the AMEs and Newman’s method, we obtain s_{max} and λ_{c2} for the case with $0 < \rho < 1$.

Let us consider the S components in a typical final state for the SIR model on an infinitely large RRG with $\rho > 0$. In the previous section, we already have the probability $s_{l,0}(\infty)$ that a randomly chosen node is susceptible and has l susceptible neighbors [$s_{l,m}(\infty) = 0$ for $m \neq 0$]. Using $s_{l,0}(\infty)$, we obtain the degree distribution of the S components as

$$p_l^s = \frac{1}{s} s_{l,0}(\infty), \quad (13)$$

where the denominator $s = \sum_{l=0}^k s_{l,0}$ is the prior probability of being susceptible. The corresponding generating function, $F_0^s(x)$, is given by

$$F_0^s(x) = \sum_{l=0}^k p_l^s x^l. \quad (14)$$

Here we assume that this subnetwork is degree uncorrelated. We consider the excess degree, which is the degree of the

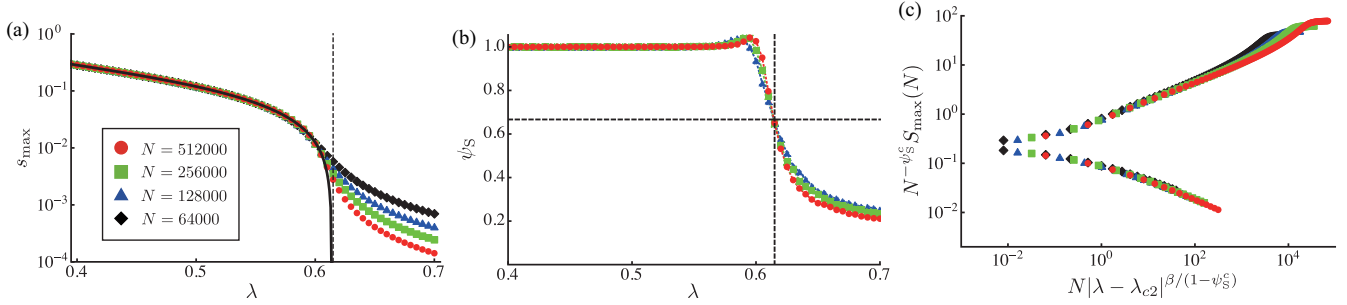


FIG. 2. (a) Fraction of the largest S component, s_{\max} , as a function of λ . Symbols were obtained from Monte Carlo simulations. The solid line was drawn by evaluating Eq. (17). (b) Numerical results of the fractal exponent of the largest S component, ψ_S . Data with several values of N have a crossing point at $\lambda_{c2} \simeq 0.615$ and $\psi_S^c \simeq 2/3$. (c) Finite-size scaling for S_{\max} around λ_{c2} . Here we set $\psi_S^c = 2/3$ and $\beta = 1$, which means that the transition at λ_{c2} belongs to the mean-field universality class.

node reached by following a randomly chosen link minus 1 [5]. The excess degree distribution, q_l^s , which is the probability that a randomly chosen link from S components points to a (susceptible) node with excess degree l , is $(l+1)p_{l+1}^s / \sum_{l'} (l'+1)p_{l'+1}^s$. Then the generating function for the excess degree distribution of the S components is

$$F_1^s(x) = \frac{F_0^{s'}(x)}{F_0^{s'}(1)}, \quad (15)$$

and the mean excess degree is given by $F_1^{s'}(1)$. By arguing the emergence of an infinitely connected component of this subnetwork (similar to [5]), we easily find that there is an infinite S component if $F_1^{s'}(1) > 1$, and thus, the percolation transition point of the S component, λ_{c2} , satisfies

$$F_1^{s'}(1) = 1. \quad (16)$$

Following [28], we also have the mean fraction of the largest S component, s_{\max} , as

$$s_{\max} = s[1 - F_0^s(v)], \quad (17)$$

where v is the solution of

$$v = F_1^s(v). \quad (18)$$

We check these estimates using Monte Carlo simulations. Figure 2(a) shows the order parameter, i.e., the fraction of the largest S component, $s_{\max}(N)$, for RRGs with several N 's. We find that the numerical results coincide with the analytical line below λ_{c2} and tend to 0 with increasing N above λ_{c2} . To numerically obtain the transition point, λ_{c2} , we introduce the fractal exponent [35]. The fractal exponent of the largest S component is defined and approximated as

$$\psi_S = \frac{d \ln S_{\max}(N)}{d \ln N} \approx \frac{\ln S_{\max}(N) - \ln S_{\max}(N/2)}{\ln N - \ln(N/2)}. \quad (19)$$

In the limit $N \rightarrow \infty$, $\psi_S = 1$ for $\lambda < \lambda_{c2}$ and $\psi_S = 0$ for $\lambda > \lambda_{c2}$, because the largest S-component size should be proportional to N for $\lambda < \lambda_{c2}$ and finite for $\lambda > \lambda_{c2}$. As shown in Fig. 2(b), numerical results for ψ_S approach $\psi_S = 1$ ($\psi_S = 0$) for $\lambda < \lambda_{c2}$ ($\lambda > \lambda_{c2}$) as N increases and have a crossing point at λ_{c2} . From numerical data, we have $\psi_S^c \equiv \psi_S(\lambda_{c2}) \simeq 2/3$ at $\lambda_{c2} \simeq 0.615$, which coincides well with our analytical estimate (vertical line in Fig. 2).

This observation is also confirmed by a finite-size scaling. As in [35], we assume a scaling form for $S_{\max}(N)$ as

$$S_{\max}(\lambda, N) = N^{\psi_S^c} f_s[N(\Delta\lambda)^{\beta/(1-\psi_S^c)}], \quad (20)$$

where $\Delta\lambda = |\lambda_{c2} - \lambda|$, β is the critical exponent related to the order parameter, $s_{\max} \propto \Delta\lambda^\beta$, and

$$f_s(x) \propto \begin{cases} \text{const} & \text{for } x \ll 1, \\ x^{1-\psi_S^c} & \text{for } x \gg 1. \end{cases} \quad (21)$$

In Fig. 2(c), our scaling shows a nice collapse with $\psi_S^c = 2/3$ and $\beta = 1$. Because ψ_S^c is related to another critical exponent τ as $\psi_S^c = (\tau - 1)^{-1}$ [35], where τ is associated with the distribution function of S components $n_S(s)$ at the critical point, $n_S(s) \propto s^{-\tau}$, these exponents mean that the percolation transition of the S components actually occurs at λ_{c2} and belongs to the mean-field universality class such that $\beta = 1$ and $\tau = 5/2$ [36].

B. Derivation of λ_{c1}

To derive λ_{c1} for the SIR model with multiple seeds, we need to calculate the connectivity of the R components generated by each seed. We should note that a percolation analysis, as in the previous subsection, using the degree distribution of the R components $r_{\ell,0}/r$ is not applicable to this case, because such an analysis ignores the condition that *each R component is connected*. To consider the connectivity of numerous R components, we use the following procedure: (i) We first calculate the probability, P_n , that the size of the R component generated by a single seed is n . (ii) For the case of $\rho > 0$, the system has numerous R components proportional to ρ . We regard each R component as a supernode. The number of nodes confined in a supernode obeys the distribution P_n , and its degree k_n is given accordingly. (iii) Then we consider a site percolation problem of supernodes. The first percolation point, λ_{c1} , is given as the critical point where the infinitely connected component of the supernodes appears.

In Appendix B, we evaluate the mean size of the R component starting from a single seed, $\langle n \rangle (= \sum_n P_n n)$, and the corresponding mean square size, $\langle n^2 \rangle (= \sum_n P_n n^2)$, by using generating functions. Then we consider the case of $\rho > 0$. Below λ_{c1} , we naturally assume that the mean size $\langle n \rangle$ is so small that each R component is a tree [37] and that any

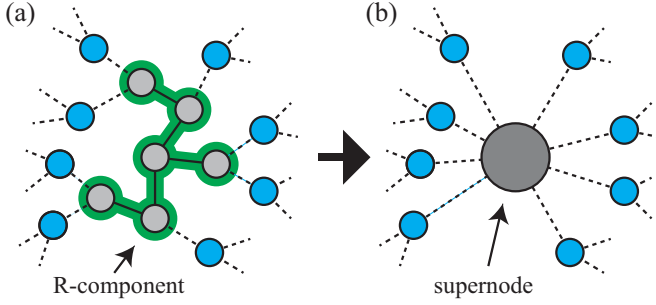


FIG. 3. Example of (a) an R component and (b) the corresponding supernode. In this example, the R component, of size $n = 6$ on a 3-RRG, has $n - 1 = 5$ edges inside (solid lines) and $zn - 2(n - 1) = 8$ edges attached to susceptible nodes (dashed lines). Thus, the degree of the supernode is $k_n = 8$.

overlaps between the R components are negligible so that the total fraction of the R components can be evaluated as $\rho \langle n \rangle$ [38], which should necessarily be less than 1. Then we can determine the creation process of the infinite R component by regarding each R component of size n as a supernode whose degree depends on n (see Fig. 3) and considering the percolation problem of these supernodes.

The density of susceptible nodes, s , is just 1 minus the density of the removed nodes, $\rho \langle n \rangle$:

$$s = 1 - \rho \langle n \rangle. \quad (22)$$

Then the probability \tilde{p} that the node reached by following a randomly chosen link is a component of a supernode is

$$\tilde{p} = \frac{\rho \langle k_n \rangle}{\rho \langle k_n \rangle + zs}, \quad (23)$$

where k_n is the number of external links of the R component (the degree of the supernode) having size n and is given by

$$k_n = (z - 2)n + 2. \quad (24)$$

Equation (24) holds since each R component is a tree with the number of edges equal to the number of nodes minus 1. The mean branching ratio of supernodes, B , is evaluated by multiplying \tilde{p} by the mean excess degree of supernodes:

$$B = \tilde{p} \frac{\langle k_n(k_n - 1) \rangle}{\langle k_n \rangle} = \frac{\rho \langle k_n(k_n - 1) \rangle}{\rho \langle k_n \rangle + zs}. \quad (25)$$

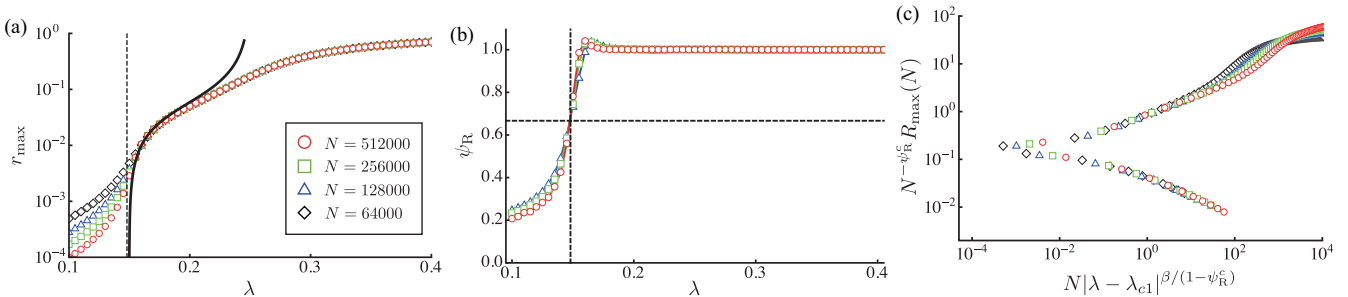


FIG. 4. (a) Fraction of the largest R component r_{\max} as a function of λ . Symbols were obtained from Monte Carlo simulations. The solid line was drawn by evaluating Eq. (C4). (b) Numerical results of the fractal exponent of the largest R component, ψ_R . Data with several values of N have a crossing point at $\lambda_{c1} \simeq 0.148$ and $\psi_R^c \simeq 2/3$. (c) Finite-size scaling for R_{\max} around λ_{c1} . Here we set $\psi_R^c = 2/3$ and $\beta = 1$, which means that the transition at λ_{c1} belongs to the mean-field universality class.

The percolation of supernodes takes place when $B \geq 1$, and thus the transition point is given by $B = 1$. That is, λ_{c1} satisfies

$$\begin{aligned} \frac{z}{\rho} &= \langle k_n(k_n - 2) \rangle + z \langle n \rangle \\ &= z_2^2 \langle n^2 \rangle + (3z - 4) \langle n \rangle, \end{aligned} \quad (26)$$

where $\langle n \rangle$ and $\langle n^2 \rangle$ are functions of λ .

We can show that these moments diverge as $\langle n \rangle \sim (\lambda_c^{\text{SIR}} - \lambda)^{-1}$ and $\langle n^2 \rangle \sim (\lambda_c^{\text{SIR}} - \lambda)^{-3}$ when λ approaches λ_c^{SIR} from below (see Appendix B), and therefore $\lambda_{c1} \rightarrow \lambda_c^{\text{SIR}}$ as $\rho \rightarrow 0$ like

$$\lambda_c^{\text{SIR}} - \lambda_{c1} \sim \rho^{1/3}. \quad (27)$$

Thus, a small increase in ρ drastically reduces λ_{c1} from λ_c^{SIR} .

We approximately have the fraction of the largest R component, r_{\max} , by applying a procedure similar to the derivation of s_{\max} to the connected components of supernodes (see Appendix C). This approximation may predict a rise of the order parameter r_{\max} around λ_{c1} but inherently overestimates r_{\max} for $\lambda > \lambda_{c1}$ due to the overlaps between the R components generated from each seed being non-negligible [see Fig. 4(a)].

We also check our estimate by comparison with Monte Carlo simulations. In Figs. 4(a) and 4(b), we plot the Monte Carlo results for the order parameter, $r_{\max}(N)$, and the corresponding fractal exponent, $\psi_R(N) \equiv d \ln r_{\max}(N) / d \ln N$. In a manner similar to that in the previous subsection, we find that the crossing point of ψ_R is at our estimate of λ_{c1} , $\lambda_{c1} \simeq 0.148$. We also find a good scaling result for $R_{\max}(N)$ using $\psi_R^c \equiv \psi_R(\lambda_{c1}) = 2/3$, $\beta = 1$, and the estimated λ_{c1} [Fig. 4(c)], supporting the validity of our estimate and indicating that the percolation transition at λ_{c1} belongs to the mean-field universality class.

C. Phase diagram

We analytically and numerically evaluate λ_{c1} and λ_{c2} for several values of ρ . In Fig. 5, we have the phase diagram of (ρ, λ) space. We find that our estimates of λ_{c1} and λ_{c2} perfectly match the Monte Carlo results. The first percolation point λ_{c1} is smaller than λ_c^{SIR} as long as $\rho > 0$. That is, the percolation of the R components occurs without global outbreaks. The gap between λ_{c1} and λ_c^{SIR} shrinks with decreasing ρ and $\lambda_{c1} = \lambda_c^{\text{SIR}}$

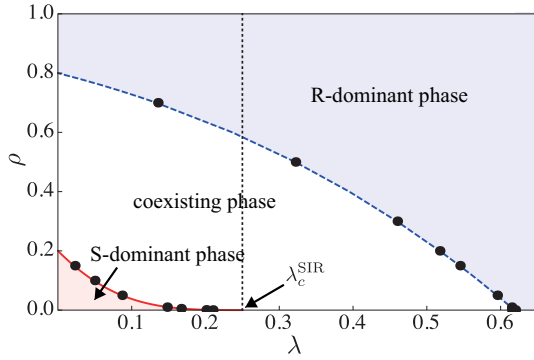


FIG. 5. Phase diagram in the (ρ, λ) space. Solid red and dashed blue lines are the analytically obtained λ_{c1} and λ_{c2} , respectively. Black circles are plotted by the crossings of ψ_R and ψ_S .

in the limit $\rho \rightarrow 0$. Note that $\lambda_{c1} = 0$ when $\rho \geq 0.2$ because the seeds themselves percolate (the site percolation threshold of the z -RRG is $1/(z-1)$, which is derived from the local tree approximation [5,6]), and $\lambda_{c2} = 0$ when $\rho \geq 0.8$ because the seeds themselves disintegrate the susceptible network into finite components.

Our finite-size scaling for several values of ρ shows that both percolation transitions at λ_{c1} and λ_{c2} belong to the mean-field universality class, irrespective of the value of ρ . This seems unsurprising because the two processes comprising the present model, the SIR model and site percolation, belong to the mean-field universality class of percolation when the graph is RRG.

When $\rho > 0$, the system does not show any singular behavior at λ_c^{SIR} . However, this does not mean that λ_c^{SIR} is unimportant. In practice, λ_c^{SIR} is still an important measure in the strategy for disease control because a single seed has the potential to induce a global outbreak above λ_c^{SIR} (in other words, the basic reproduction number $R_0 > 1$ when $\lambda > \lambda_c^{\text{SIR}}$). The singular behaviors at λ_{c1} , e.g., the divergence of the R susceptibility, may be interpreted as a precursor to global outbreaks, like the proverbial canary in a coal mine.

D. SIR model in regular lattices

We have numerically and analytically shown that the present model with multiple seeds on the RRG percolates at a lower infection rate than the epidemic threshold. Is this phenomenon in common with other networks, e.g., networks with many short loops and without the logarithmic dependence of the mean shortest path? In the rest of this section, we briefly consider the SIR model with multiple seeds on finite-dimensional Euclidean lattices by Monte Carlo simulations.

First, we consider the cubic lattice with the periodic boundary condition. In Monte Carlo simulations, we set $\mu = 1$, $\rho = 0.01$, and $N = 40^3, 50^3, 60^3, 70^3$. The number of trials is 50 000. In Fig. 6(a), we show the size dependence of the order parameters, r_{max} and s_{max} . We find that r_{max} and s_{max} become nonzero and 0 at different points $\lambda_{c1} \simeq 0.27$ and $\lambda_{c2} \simeq 0.49$, respectively. This discrepancy is also led by the peak positions of R susceptibility and S susceptibility, as shown in Fig. 6(b). Both λ_{c1} and λ_{c2} are also different from the epidemic threshold λ_c^{SIR} , which is obtained from the single-seed simulations (not shown). Starting from a single seed, $r_{\text{max}} (= r)$ becomes nonzero at $\lambda_c^{\text{SIR}} \simeq 0.36$, which is larger than λ_{c1} . Then we have the discrepancy among λ_{c1} , λ_c^{SIR} , and λ_{c2} , on the cubic lattice, and expect that the observed phenomena on the RRG will hold for other clustered networks. A qualitative difference between the cubic lattice and the RRG is in their universality class. From the crossings of the fractal exponents ψ_R and ψ_S , we have $\psi_R^c \simeq \psi_S^c \simeq 0.84$ for the cubic lattice (not shown), and this estimate means that transitions of both R components and S components belong to the universality class of three-dimensional percolation transition [36] but not to the mean-field universality class.

Let us mention a special case, the SIR model in the square lattice with the periodic boundary condition. In Fig. 7, we show the Monte Carlo results. In this case, s_{max} and r_{max} seem to undergo a macroscopic change at the same point, i.e., $\lambda_{c1} = \lambda_{c2} \simeq 0.91$ [see Fig. 7(a)]. The corresponding susceptibilities also seem to have a peak at the same value of λ [Fig. 7(b)]. Compared to single-seed simulations, λ_{c1} and λ_{c2} decrease with an increase in ρ and differ from the epidemic threshold $\lambda_c^{\text{SIR}} \simeq 1.17$. The absence of the coexisting phase

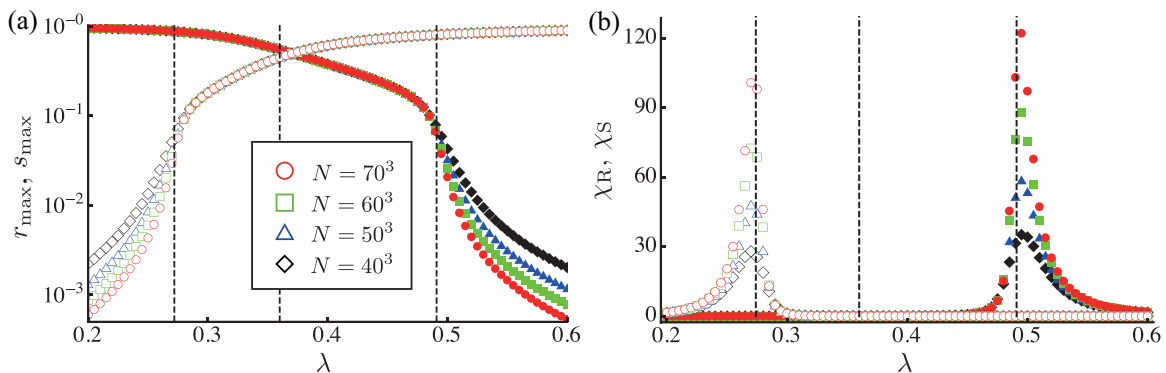


FIG. 6. Monte Carlo results for the SIR model on a cubic lattice with the periodic boundary condition: (a) fractions of the largest R component (open symbols) and of the largest S component (filled symbols), r_{max} and s_{max} ; (b) R susceptibility (open symbols) and S susceptibility (filled symbols), χ_R and χ_S . The three vertical lines represent λ_{c1} , λ_c^{SIR} , and λ_{c2} , from left to right. Here $\lambda_{c1} \simeq 0.27$ and $\lambda_{c2} \simeq 0.49$ were confirmed by the crossings of ψ_R and ψ_S and their finite-size scalings, and $\lambda_c^{\text{SIR}} \simeq 0.36$ was obtained from the Monte Carlo simulations for the SIR model with a single seed (not shown).

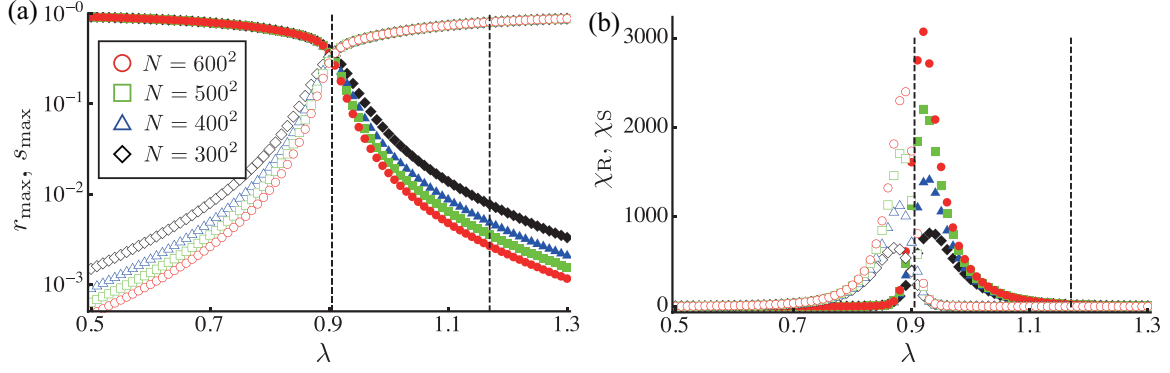


FIG. 7. Monte Carlo results for the SIR model on a square lattice with the periodic boundary condition: (a) fractions of the largest R component (open symbols) and of the largest S component (filled symbols), r_{\max} and s_{\max} ; (b) R susceptibility (open symbols) and S susceptibility (filled symbols), χ_R and χ_S . In these simulations, we set $\mu = 1$, $\rho = 0.01$, and $N = 300^2, 400^2, 500^2, 600^2$. Each of data is averaged over 50 000 trials. The two vertical lines represent $\lambda_{c1} = \lambda_{c2} \simeq 0.91$ (left) and $\lambda_c^{\text{SIR}} \simeq 1.17$ (right), respectively. Here $\lambda_{c1} = \lambda_{c2}$ was confirmed by the crossings of ψ_R and ψ_S and their finite-size scalings, and λ_c^{SIR} was obtained from the Monte Carlo simulations for the SIR model with a single seed (not shown).

does not seem surprising if we consider a spatial constraint of the square lattice: When the largest component percolates the lattice vertically and horizontally, the residual components after removing the largest one cannot maintain the connection across the lattice. (This reflects on the fact that the percolation threshold is equal to or larger than $1/2$ in both site and bond percolations.) Turning to other real spatial networks, which are often regarded as two-dimensional objects, it is an open question whether or not the coexisting phase exists.

V. SUMMARY

In this paper, we have studied the SIR model in an RRG with a nontrivial fraction of infection seeds, ρ . Through analytical estimates and numerical simulations, we have obtained the phase diagram in (ρ, λ) space. The SIR model with numerous seeds shows the percolation transition of the removed and susceptible nodes at λ_{c1} and λ_{c2} , respectively. In particular, λ_{c1} is smaller than the epidemic threshold λ_c^{SIR} as long as $\rho > 0$. This means that epidemic clusters generated by multiple seeds percolate without global outbreaks.

So far, we have focused on the SIR model in the RRG and the lattices. We expect that the above statement holds for the SIR model in other networks, although the details of the phase transition may depend on network structures, e.g., $\lambda_{c1} < \lambda_c^{\text{SIR}} = 0$ in a fat-tailed scale-free network with $\gamma \leq 3$.

Finally, we briefly discuss other epidemic models with multiple seeds. Krapivsky *et al.* [39] proposed an extended SIR model, called a transient fad, with the assumption of a well-mixed population. They analytically showed that this model exhibits a discontinuous transition if $\rho > 0$. The authors and a collaborator [40] performed Monte Carlo simulations for this fad model in networks to confirm that a discontinuous jump of the order parameter appears near the epidemic threshold, which is behind the percolation of epidemic clusters. The authors also investigated the discrete-time version of the transient fad to confirm it numerically and analytically [41]. Very recently, several generalized epidemic models in networks beyond the classical SIR model have

been investigated [42–45]. It will be interesting to clarify what numerous seeds induce in such generalized epidemic models.

ACKNOWLEDGMENTS

T.H.'s work was partially supported by Grant-in-Aid for Young Scientists (B) (Nos. 24740054 and 15K17716) and Grant-in-Aid for Scientific Research (B) (No. 26310203) from the Japan Society for the Promotion of Science (JSPS), and by JST, ERATO, Kawarabayashi Large Graph Project.

APPENDIX A: DERIVATION OF λ_c^{SIR} FOR THE LIMIT $\rho \rightarrow 0$

The AMEs do not predict any transition point when $\rho > 0$ because $r > \rho > 0$. However, it is possible to derive the transition point λ_c^{SIR} if the fraction of infection seeds is infinitesimally small ($\rho \rightarrow 0$). In the AMEs for $\{s_{l,m}\}$, only $s_{z,0}$ and $s_{z-1,1}$ are relevant up to the first order of ρ ,

$$\begin{aligned} \dot{s}_{z,0} &= -\beta_s^{si} z s_{z,0}, \\ \dot{s}_{z-1,1} &= -\lambda s_{z-1,1} + \beta_s^{si} z s_{z,0} - \beta_s^{ir} s_{z-1,1}, \end{aligned} \quad (\text{A1})$$

with

$$\beta_s^{si} = \lambda \frac{(z-1)s_{z-1,1}}{z s_{z,0}}, \quad \beta_s^{ir} = \mu, \quad (\text{A2})$$

and the initial condition

$$s_{z,0}(0) = 1 - (z+1)\rho, \quad s_{z-1,1}(0) = z\rho. \quad (\text{A3})$$

Equation (A2) is substituted into Eq.(A1) to find the condition for $s_{z-1,1}$ to remain finite as $t \rightarrow \infty$,

$$\frac{\mu}{\lambda} > z - 2, \quad (\text{A4})$$

and thus, the lower bound of μ/λ gives the epidemic threshold, $\lambda_c^{\text{SIR}} = \mu/(z-2)$, which corresponds to the known result, (1).

APPENDIX B: DISTRIBUTION OF THE R COMPONENT GENERATED FROM A SINGLE SEED

First, we evaluate the size distribution of the R component created by a single seed. To do this, we need to know the probability, $p_\ell^{(k)}$, that an infected node will infect ℓ of k neighboring susceptible nodes before being removed. Such an infected node is removed before infecting any neighbors with a probability $p_0^{(k)} = \frac{1}{1+k\lambda}$, so that the probability of its infecting at least one neighboring node before removal is $1 - p_0^{(k)} = \frac{k\lambda}{1+k\lambda}$. As shown in Fig. 8, we can express $p_\ell^{(k)}$ as a recursive form,

$$p_\ell^{(k)} = \begin{cases} \frac{1}{1+k\lambda}, & \ell = 0, \\ \frac{k\lambda}{1+k\lambda} \times p_{\ell-1}^{(k-1)}, & 0 < \ell \leq k. \end{cases} \quad (\text{B1})$$

From this equation, we find that the generating function of $p_\ell^{(k)}$,

$$g_k(x) = \sum_{\ell=0}^k p_\ell^{(k)} x^\ell, \quad (\text{B2})$$

satisfies the recursion relation

$$g_k(x) = \frac{1 + k\lambda x g_{k-1}(x)}{1 + k\lambda} \quad (\text{B3})$$

with $g_0(x) = 1$.

Now let P_n be the probability that a single seed creates an R component of size n , and let Q_n be the probability that a node infected by another node further creates a partial R component of size n . Then, by considering the infection process starting

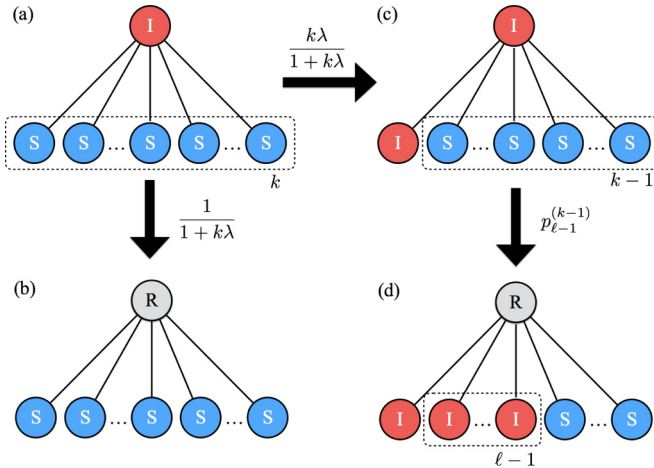


FIG. 8. Schematic of the recursive relation for $p_\ell^{(k)}$. Let consider the probability $p_\ell^{(k)}$ that an infected node infects ℓ nodes of k susceptible neighbors before being removed [(a)→(d)]. The probability that this infected node is removed before infecting any neighbors [(a)→(b)] is $p_0^{(k)} = 1/(1+k\lambda)$. On the other hand, the event that this node infects one susceptible neighbor [(a)→(c)] occurs with probability $1 - p_0^{(k)} = k\lambda/(1+k\lambda)$. At (c), the focal infected node infects further $\ell - 1$ nodes from $k - 1$ remaining neighbors before being removed [(c)→(d)] with probability $p_{\ell-1}^{(k-1)}$ because the infecting process is Markovian. Thus, $p_\ell^{(k)}$, which is the probability from (a) to (d), is given as $p_{\ell-1}^{(k-1)} \times k\lambda/(1+k\lambda)$.

from a single seed, P_n can be evaluated as

$$P_n = \sum_{\ell=0}^z p_\ell^{(z)} \sum_{m_1, m_2, \dots, m_\ell} Q_{m_1} Q_{m_2} \dots Q_{m_\ell} \delta_{n, 1 + \sum_{\mu=0}^{\ell} m_\mu}, \quad (\text{B4})$$

and similarly, Q_n can be recursively given as

$$Q_n = \sum_{\ell=0}^{z_1} p_\ell^{(z_1)} \sum_{m_1, m_2, \dots, m_\ell} Q_{m_1} Q_{m_2} \dots Q_{m_\ell} \delta_{n, 1 + \sum_{\mu=0}^{\ell} m_\mu}, \quad (\text{B5})$$

where $z_\nu = z - \nu$ (Fig. 9). Introducing the corresponding generating functions,

$$G_0(x) = \sum_{n=1}^{\infty} P_n x^n, \quad G_1(x) = \sum_{n=1}^{\infty} Q_n x^n, \quad (\text{B6})$$

we can express the above relations (B4) and (B5) in a compact form as

$$G_0(x) = x g_z(G_1(x)) \quad (\text{B7})$$

and

$$G_1(x) = x g_{z_1}(G_1(x)), \quad (\text{B8})$$

respectively.

What we want to know is the mean size of the R component, $\langle n \rangle = G'_0(1)$, and the mean square size of the R component, $\langle n^2 \rangle = G''_0(1) + G'_0(1)$. To evaluate these values, we need the derivative of $g_k(x)$, which is given by

$$g'_k(x) = \frac{k\lambda}{1+k\lambda} [g_{k-1}(x) + x g'_{k-1}(x)], \quad (\text{B9})$$

from which the mean value $\langle \ell \rangle_k$ is easily found to be

$$\langle \ell \rangle_k = g'_k(1) = \frac{k\lambda}{1+\lambda}. \quad (\text{B10})$$

One also requires the second derivative,

$$g''_k(x) = \frac{k\lambda}{1+k\lambda} [2g'_{k-1}(x) + x g''_{k-1}(x)], \quad (\text{B11})$$

so that

$$\langle \ell(\ell-1) \rangle_k = g''_k(1) = \frac{2k(k-1)\lambda^2}{(1+\lambda)(1+2\lambda)}, \quad (\text{B12})$$

yielding

$$\langle \delta \ell^2 \rangle_k = \langle \ell^2 \rangle_k - \langle \ell \rangle_k^2 = \frac{k\lambda[1 + (k+1)\lambda]}{(1+\lambda)^2(1+2\lambda)}. \quad (\text{B13})$$

Now we can evaluate the derivatives of $G_0(x)$ and $G_1(x)$ as

$$G'_0 = g'_z(G_1) + x g'_z(G_1) G'_1, \quad (\text{B14})$$

$$G''_0 = 2g'_z(G_1) G'_1 + x g''_z(G_1) G_1^2 + x g'_z(G_1) G''_1 \quad (\text{B15})$$

and

$$G'_1 = g_{z_1}(G_1) + x g'_{z_1}(G_1) G'_1, \quad (\text{B16})$$

$$G''_1 = 2g'_{z_1}(G_1) G'_1 + x g''_{z_1}(G_1) G_1^2 + x g'_{z_1}(G_1) G''_1. \quad (\text{B17})$$

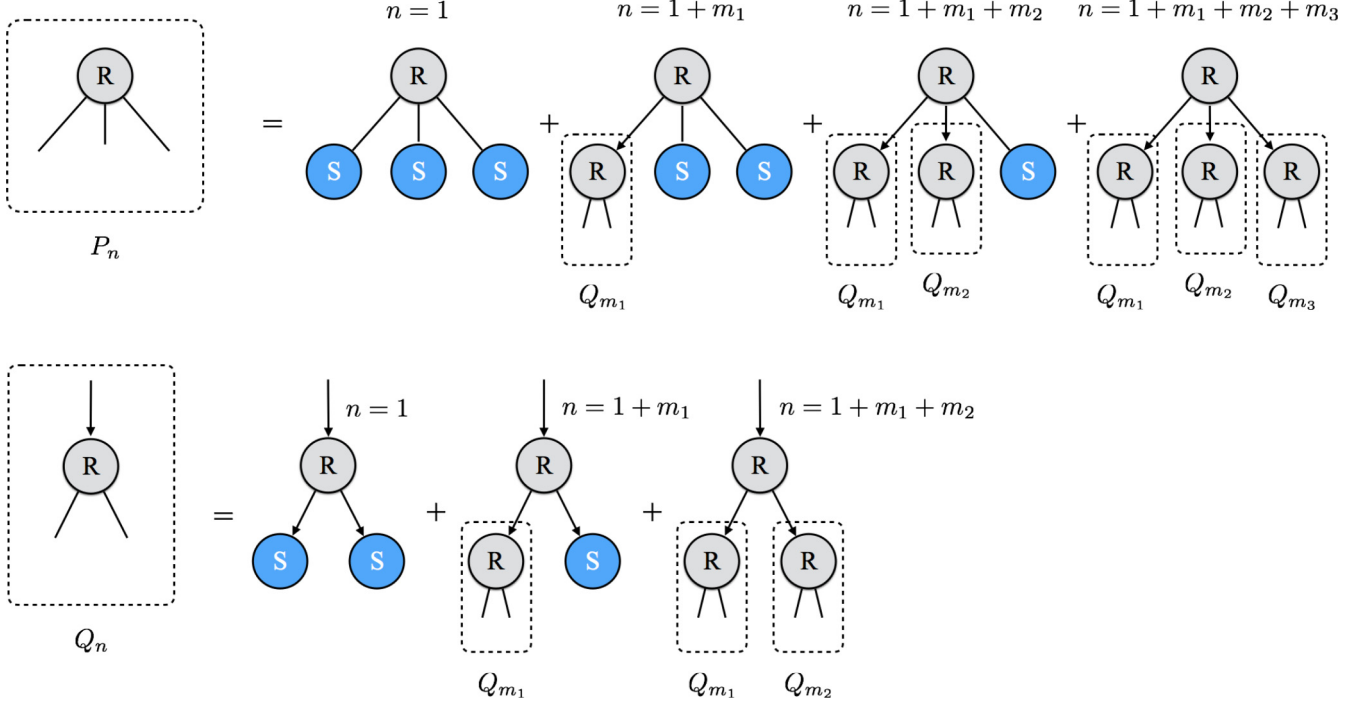


FIG. 9. Schematic of P_n (top) and Q_n (bottom) for the case of the RRG with $z = 3$: $P_n = p_0^{(3)}\delta_{n,1} + p_1^{(3)}\sum_{m_1} Q_{m_1}\delta_{n,1+m_1} + p_2^{(3)}\sum_{m_1,m_2} Q_{m_1}Q_{m_2}\delta_{n,1+m_1+m_2} + p_3^{(3)}\sum_{m_1,m_2,m_3} Q_{m_1}Q_{m_2}Q_{m_3}\delta_{n,1+m_1+m_2+m_3}$ and $Q_n = p_0^{(2)}\delta_{n,1} + p_1^{(2)}\sum_{m_1} Q_{m_1}\delta_{n,1+m_1} + p_2^{(2)}\sum_{m_1,m_2} Q_{m_1}Q_{m_2}\delta_{n,1+m_1+m_2}$.

Setting $x = 1$ gives $G_1(1) = 1$ and

$$G'_1(1) = 1 + g'_{z_1}(1)G'_1(1) = \frac{1}{1 - g'_{z_1}(1)} = \frac{1}{1 - \langle \ell \rangle_{z_1}}, \quad (\text{B18})$$

$$\begin{aligned} G''_1(1) &= 2g'_{z_1}(1)G'_1(1) + g''_{z_1}(1)G'_1(1)^2 + g'_{z_1}(1)G''_1(1) \\ &= G'_1(1)^3 [2g'_{z_1}(1)(1 - g'_{z_1}(1)) + g''_{z_1}(1)]. \end{aligned} \quad (\text{B19})$$

These quantities provide an explicit expression for the first moment, M_1 , and the second cumulant, C_2 (and thus the second moment $M_2 = C_2 + M_1^2$), of P_n as

$$M_1 = \langle n \rangle = G'_0(1) = 1 + \langle \ell \rangle_z G'_1(1), \quad (\text{B20})$$

$$\begin{aligned} C_2 &= \langle n^2 \rangle - \langle n \rangle^2 \\ &= G''_0(1) + M_1 - M_1^2 \\ &= G'_1(1)^2 [g''_{z_1}(1) + g'_z(1) - g'_{z_1}(1)^2] \\ &\quad + g'_z(1) [G'_1(1) + G'_1(1) - G'_1(1)^2] \\ &= G'_1(1)^2 \langle \delta \ell^2 \rangle_z + G'_1(1)^3 \langle \ell \rangle_z \langle \delta \ell^2 \rangle_{z_1}. \end{aligned} \quad (\text{B21})$$

When λ approaches λ_c^{SIR} from below, $G'_1(1)$ dominates the behavior of M_1 and C_2 . Indeed (B18) tells us that $G'_1(1)$ diverges as $\delta\lambda^{-1}$, where $\delta\lambda = \lambda_c^{\text{SIR}} - \lambda$, and thus

$$M_1 = \langle n \rangle \sim \delta\lambda^{-1}, \quad C_2 \sim \langle n^2 \rangle \sim \delta\lambda^{-3}. \quad (\text{B22})$$

Substituting Eq. (B22) for Eq. (26), we have a power-law dependence of the gap $\delta\lambda$ on the seed fraction ρ as Eq. (27).

APPENDIX C: LARGEST R-COMPONENT SIZE

The generating function of the probability that a supernode will have the degree k_n is given by

$$H_0(x) = \sum_{n=1}^{\infty} P_n x^{k_n} = x^2 G_0(x^{z_2}), \quad (\text{C1})$$

and that of the excess degree as

$$H_1(x) = \frac{H'_0(x)}{H'_0(1)} = \frac{2xG_0(x^{z_2}) + z_2 x^{z_1} G'_0(x^{z_2})}{\langle k_n \rangle}. \quad (\text{C2})$$

Let u be the probability that a finite cluster of supernodes is found by following randomly chosen links; this satisfies

$$u = 1 - \tilde{p} + \tilde{p}H_1(u). \quad (\text{C3})$$

Here, \tilde{p} is the probability that the node reached by following a randomly chosen link is a component of a supernode and is given by Eq. (23). Then, the density of the largest component of supernodes in size, i.e., r_{max} , is evaluated as

$$r_{\text{max}} = \rho \sum_{n=1}^{\infty} n P_n (1 - u^{k_n}) = \rho [\langle n \rangle - u^z G'_0(u^{z_2})], \quad (\text{C4})$$

where we have used $\langle k_n \rangle = (z - 2)\langle n \rangle + 2$ from Eq. (24).

- [1] W. O. Kermack and A. G. McKendrick, *Proc. R. Soc. London A: Math. Phys. Eng. Sci.* **115**, 700 (1927).
- [2] R. M. Anderson and R. M. May, *Infectious Diseases of Humans: Dynamics and Control* (Oxford University Press, New York, 1992).
- [3] R. Pastor-Satorras, C. Castellano, P. Van Mieghem, and A. Vespignani, *Rev. Mod. Phys.* **87**, 925 (2015).
- [4] R. Albert and A.-L. Barabási, *Rev. Mod. Phys.* **74**, 47 (2002).
- [5] M. E. J. Newman, *SIAM Rev.* **45**, 167 (2003).
- [6] S. N. Dorogovtsev, A. V. Goltsev, and J. F. F. Mendes, *Rev. Mod. Phys.* **80**, 1275 (2008).
- [7] A. Barrat, M. Barthélemy, and A. Vespignani, *Dynamical Processes on Complex Networks* (Cambridge University Press, Cambridge, UK, 2008).
- [8] Y. Moreno, R. Pastor-Satorras, and A. Vespignani, *Eur. Phys. J. B* **26**, 521 (2002).
- [9] P. Grassberger, *Math. Biosci.* **63**, 157 (1983).
- [10] M. E. J. Newman, *Phys. Rev. E* **66**, 016128 (2002).
- [11] J. C. Miller, A. C. Slim, and E. M. Volz, *J. R. Soc. Interface* **9**, 890 (2012).
- [12] J. Lindquist, J. Ma, P. Van den Driessche, and F. H. Willeboordse, *J. Math. Biol.* **62**, 143 (2011).
- [13] J. P. Gleeson, *Phys. Rev. Lett.* **107**, 068701 (2011).
- [14] J. P. Gleeson, *Phys. Rev. X* **3**, 021004 (2013).
- [15] R. Pastor-Satorras and A. Vespignani, *Phys. Rev. E* **65**, 036104 (2002).
- [16] N. Madar, T. Kalisky, R. Cohen, D. ben-Avraham, and S. Havlin, *Eur. Phys. J. B* **38**, 269 (2004).
- [17] L. K. Gallos, F. Liljeros, P. Argyrakis, A. Bunde, and S. Havlin, *Phys. Rev. E* **75**, 045104 (2007).
- [18] R. Cohen, S. Havlin, and D. ben-Avraham, *Phys. Rev. Lett.* **91**, 247901 (2003).
- [19] P. Holme, *Europhys. Lett.* **68**, 908 (2004).
- [20] Y. Chen, G. Paul, S. Havlin, F. Liljeros, and H. E. Stanley, *Phys. Rev. Lett.* **101**, 058701 (2008).
- [21] J. C. Miller, *PLoS ONE* **9**, e101421 (2014).
- [22] Z.-L. Hu, J.-G. Liu, G.-Y. Yang, and Z.-M. Ren, *Europhys Lett.* **106**, 18002 (2014).
- [23] S. Ji, L. Lu, C. H. Yeung, and Y. Hu, [arXiv:1508.04294](https://arxiv.org/abs/1508.04294).
- [24] Here we replaced the transmissibility T in [10] with λ as $T = \lambda/(\mu + \lambda)$ with $\mu = 1$. In [10], the transmissibility T is given as $T = \langle T_{ij} \rangle = 1 - \int_0^\infty dr d\tau P(r)P(\tau)e^{-r\tau}$, where T_{ij} is the probability that the disease did not transmit from node i to node j before node i was removed when we consider the pair of an infected node i and a susceptible node j , r is the infection rate between the focal pair, τ is the time for which the infected node remains infected, and $P(r)$ and $P(\tau)$ are the corresponding distributions. In the present case, we have $P(r) = \delta(r - \lambda)$ (because the infection rate is a constant λ), $P(\tau) = \mu e^{-\mu\tau}$ (as the distribution of the interevent time of a Poisson process with parameter μ), and $T = 1 - \int_0^\infty dr d\tau \delta(r - \lambda) \mu e^{-\mu\tau} e^{-r\tau} = 1 - \mu \int_0^\infty d\tau e^{-(\mu+\lambda)\tau} = \lambda/(\mu + \lambda)$.
- [25] E. Kenah and J. C. Miller, *Interdiscip. Perspect. Infect. Dis.* **2011**, 543520 (2011).
- [26] T. Tomé and R. M. Ziff, *Phys. Rev. E* **82**, 051921 (2010).
- [27] D. R. de Souza, T. Tomé, and R. M. Ziff, *J. Stat. Mech.: Theory Exp.* (2011) P03006.
- [28] M. E. J. Newman, *Phys. Rev. Lett.* **95**, 108701 (2005).
- [29] M. J. Ferrari, S. Bansal, L. A. Meyers, and O. N. Björnstad, *Proc. R. Soc. London B* **273**, 2743 (2006).
- [30] S. Bansal and L. A. Meyers, *J. Theor. Biol.* **309**, 176 (2012).
- [31] L. D. Valdez, P. A. Macri, and L. A. Braunstein, *Phys. Rev. E* **85**, 036108 (2012).
- [32] T. Hasegawa and N. Masuda, *J. Stat. Mech.: Theory Exp.* (2011) P09014.
- [33] T. Hasegawa, K. Konno, and K. Nemoto, *Eur. Phys. J. B* **85**, 1 (2012).
- [34] The susceptibilities χ_R and χ_S are given as $\chi_R = \sum_{r \neq r_{\max}} r^2 n_R(r)$ and $\chi_S = \sum_{s \neq s_{\max}} s^2 n_S(s)$, where $n_R(r)$ [$n_S(s)$] means the mean number of R components [S components] of size r [s] per node.
- [35] T. Hasegawa, T. Nogawa, and K. Nemoto, *Europhys. Lett.* **104**, 16006 (2013).
- [36] D. Stauffer and A. Aharony, *Introduction to Percolation Theory* (Taylor and Francis, London, 1994).
- [37] Finite components have no cyclic path in infinite locally treelike networks.
- [38] This condition means that the total size of the R components is smaller than the number of nodes. Let us consider a finite network with N nodes. The number of seeds is $N\rho$, and the mean R-component size for each seed is $\langle n \rangle$. Then the total size of the R components is $N\rho\langle n \rangle$. Therefore, our assumption in the main text is equivalent to the statement that $N\rho\langle n \rangle < N$.
- [39] P. L. Krapivsky, S. Redner, and D. Volovik, *J. Stat. Mech.: Theory Exp.* (2011) P12003.
- [40] T. Hasegawa, N. Kinoshita, and K. Nemoto (unpublished) (2016).
- [41] T. Hasegawa and K. Nemoto, *J. Stat. Mech.: Theory Exp.* (2014) P11024.
- [42] G. Bizhani, M. Paczuski, and P. Grassberger, *Phys. Rev. E* **86**, 011128 (2012).
- [43] K. Chung, Y. Baek, D. Kim, M. Ha, and H. Jeong, *Phys. Rev. E* **89**, 052811 (2014).
- [44] W. Cai, L. Chen, F. Ghanbarnejad, and P. Grassberger, *Nature Phys.* **11**, 936 (2015).
- [45] J. Gómez-Gardeñes, A. S. de Barros, S. T. Pinho, and R. F. Andrade, *Europhys. Lett.* **110**, 58006 (2015).